Available online at www.sciencedirect.com
ScienceDirect
Thin Solid Films 516 (2008) 8013 – 8021
www.elsevier.com/locate/tsf

Polychromatic X-ray micro- and nanodiffraction for spatially-resolved structural studies

J.D. Budai [a,*], W. Liu [b], J.Z. Tischler [a], Z.W. Pan [c], D.P. Norton [d], B.C. Larson [a], W. Yang [e], G.E. Ice [a]

[a] *Materials Science & Technology, Oak Ridge National Laboratory, Oak Ridge, TN, United States*
[b] *Advanced Photon Source, Argonne National Laboratory, Argonne, IL, United States*
[c] *Physics and Engineering, University of Georgia, Athens, GA, United States*
[d] *Materials Science & Engineering, University of Florida, Gainesville, FL, United States*
[e] *HPCAT, Geophysical Lab, Carnegie Institution of Washington, Argonne, IL, United States*

Available online 12 April 2008

Abstract

The availability of intense, focused synchrotron X-ray microbeams has enabled new techniques for materials investigations with sub-micron spatial resolution. The scanning microbeam setup we have developed at the XOR-UNI beamline at the Advanced Photon Source (APS) is versatile in that it provides 1D, 2D or 3D scans (including depth resolution), and can alternate between polychromatic- and monochromatic-beam modes. Focusing in both modes uses elliptical Kirkpatrick–Baez (K–B) reflecting mirrors. Beam diameters of ~500 nm FWHM are now routine, and 90 nm focus has been demonstrated. In white-beam mode, a CCD detector records a complete Laue diffraction pattern, which is analyzed with an automated indexing program. These X-ray diffraction patterns provide real-space maps of the local lattice structure, crystal orientation, grain morphology, and strain tensor.

Spatially-resolved X-ray microdiffraction studies are now providing previously unavailable measurements of local microstructures. These measurements, in turn, yield new insights in several classic fields of materials science. This paper will illustrate the application of polychromatic scanning X-ray microscopy with examples from 1D, 2D and 3D materials systems. In 1D systems, we have mapped the structure and orientation of an individual ZnO nanorod along with the associated Ge catalyst particle used to control the nanocrystal growth. In 2D systems, X-ray microdiffraction studies have revealed the mechanisms for local crystallographic tilting in epitaxial oxide films grown on textured Ni substrates for superconducting applications. In 3D systems, X-ray microscopy investigations have included *in-situ* studies of microstructural evolution during thermal grain growth in polycrystalline aluminum. In general, these spatially-resolved measurements provide important new insights and are valuable as input for theoretical and computer modeling studies of a wide range of material processes.
© 2008 Elsevier B.V. All rights reserved.

Keywords: Microbeams; Polychromatic microdiffraction; Nanodiffraction; 3D X-ray microscopy; Nanostructures

1. Introduction

Material properties are often controlled by interactions between heterogeneities, i.e. between regions containing different local microstructures. For example, understanding how the size, shape and orientation of interacting polycrystalline grains affects properties such as strength is central to thermomechanical processing in metallurgy. Although X-ray diffraction has long been an important structural characterization tool, most X-ray measurements either employ large beams that average over many polycrystal grains or are obtained from single-crystal samples. Unlike electron-probe studies, spatially-resolved X-ray diffraction studies of individual grains or domains have generally been rare. The advent of high-brightness, third generation synchrotron sources and improvements in X-ray focusing optics are changing this situation. The ongoing development of X-ray imaging and spatially-resolved probes has included progressively smaller beam sizes and increasingly sophisticated techniques for making use of the

* Corresponding author. P.O. Box 2008, Oak Ridge, TN 37831-6118, United States. Tel.: +1 865 576 6721; fax: +1 865 574 7659.
E-mail address: budaijd@ornl.gov (J.D. Budai).

0040-6090/$ - see front matter © 2008 Elsevier B.V. All rights reserved.
doi:10.1016/j.tsf.2008.04.045

unique properties of synchrotron sources. The various techniques for focusing X-rays to produce small beams include Fresnel zone plates, tapered capillaries, Kirkpatrick–Baez (K–B) mirrors and compound refractive lenses [1,2]. Using the advances in X-ray optics, a range of complementary three-dimensional (3D) X-ray microscopy techniques are being developed, including approaches based on either monochromatic or polychromatic beams, coherent or incoherent radiation, and full-field or scanning imaging [2–7]. In this paper, we first describe the 3D scanning X-ray microscopy technique we have developed and then illustrate the application of polychromatic X-ray microscopy with examples from 1D, 2D and 3D material systems.

At the XOR-UNI beamline 34ID at the Advanced Photon Source (APS), we have developed a scanning, polychromatic (white) microdiffraction facility with 3D submicron spatial resolution. As shown schematically in Fig. 1, the X-ray source is broad-spectrum synchrotron radiation from an APS undulator. A double-crystal monochromator mounted on a translation stage can be moved out of or into the beam in order to select either polychromatic mode or monochromatic operation. A crossed pair of high-precision, elliptically-figured K–B mirrors then focus the beam non-dispersively onto the sample. The typical beam diameter during routine operation is ~0.5 μm FWHM. The energy spectrum covers the range from ~8–22 keV due to absorption at low energy and the mirror reflectivity at high energy. A CCD area detector measures the diffracted X-ray beams which have energies that satisfy Bragg's Law. In white beam mode, the Laue diffraction pattern typically contains a large number of peaks, with ~10–20 reflections for a single crystallite with a small unit cell and more peaks for larger unit cells. Automatic analysis software locates peaks, indexes the pattern, and calculates the local crystallographic orientation and deviatoric strain tensor information (relative lattice parameters) [6]. If an absolute measurement of the lattice parameters (dilatational strain) is desired, the monochromator is inserted and scanned through the peak energy. For thin samples such as nanostructures or films, the incident X-ray beam yields a single-crystal Laue pattern as long as the grain size is larger than the beam diameter. In this case, a white beam measurement at each location provides the local lattice structure, orientation and strain. Sample translations are then used to generate 2D orientation and strain maps. X-ray microdiffraction orientation maps are conceptually very similar to the orientation maps produced by electron backscatter diffraction (EBSD) techniques [8–10]. Generally, X-ray microdiffraction yields measurements with greater angular resolution (~0.01°) and strain resolution ($\Delta d/d \sim 10^{-4}$). X-ray beams also penetrate deeper into bulk samples than electrons, and scattering arising from different depths must be considered.

As the X-ray microbeam penetrates a bulk, polycrystalline sample, scattering can originate from many crystal grains with different orientations. The white beam pattern will consist of the superposition of many different Laue patterns. Even if an image with superimposed patterns can be indexed, the position of different grains is not known. To address this uncertainty, a differential-aperture X-ray microscopy (DAXM) technique has been developed with submicron spatial resolution along the direction of the incident beam [6,11]. As shown in Fig. 1, a series of Laue images are measured as a Pt wire is translated in small steps close to the sample surface. The wire acts as a knife-edge profiler, and difference between successive images enables a unique reconstruction of the Laue diffraction patterns for each submicron volume element (voxel) along the incident beam path. This approach yields full point-to-point structural information for every voxel, and the cost is the time required to scan the Pt wire across the surface (typically ~300 images). The reconstructed Laue patterns for each voxel are then analyzed as for the 2D situation to generate orientation and strain maps for 3D volumes inside polycrystalline materials. The 3D X-ray microscopy approach is general; the full diffraction pattern for each voxel is uniquely determined for any material that scatters X-rays. In the following sections, we illustrate how X-ray microdiffraction can be used to obtain unique structural information and new insight for different classes of materials: 1D, 2D and 3D systems.

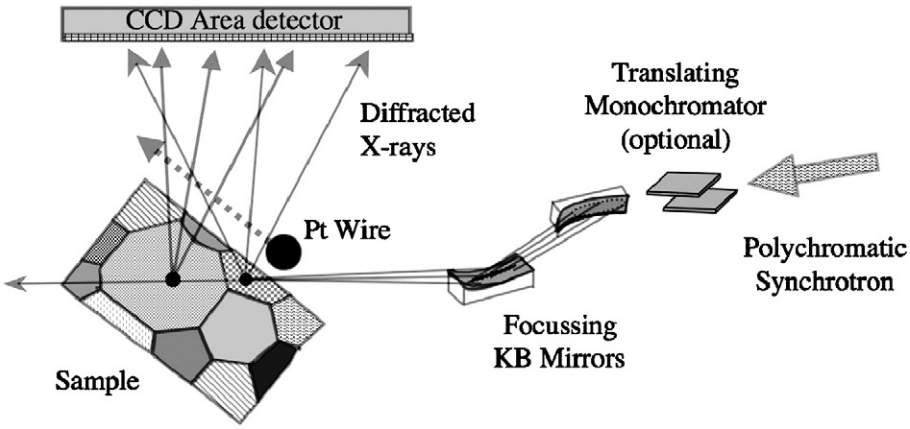

Fig. 1. Schematic drawing of the polychromatic 3D X-ray microscope at the APS beamline 34ID. Polychromatic undulator radiation is focused to a submicron beam size by a crossed pair of K–B mirrors. Diffracted beams are measured using a CCD area detector. A double-crystal monochromator can be inserted (monochromatic mode) or removed (polychromatic mode).

2. 1D: individual nanostructures

Recent advances in X-ray focusing provide new opportunities for nanoscience research. The ability to focus intense X-ray beams to increasingly smaller sizes means that X-ray scattering measurements can now be obtained from individual nanostructures. Spatially-resolved results provide more detailed information than measurements from an ensemble of many nanostructures for several reasons. For example, it is now possible to map anisotropic strain or microstructural changes such as domain boundaries along the length of a single nanowire. In addition, size-dependent properties are of great interest, and focused beams enable studies of a range of nanostructures with different dimensions from a single sample that contains a dispersion of sizes.

Several research groups have recognized the benefits of characterizing small, localized areas of nanostructures, and synchrotron beamline facilities are being developed worldwide to enable nanoscience investigations. Xiao et al. [12] describe nanodiffraction instrumentation developed on beamline 21D at the APS. This facility uses a hard X-ray Fresnel zone plate with a focal length of ~10 cm to focus a monochromatic beam to a diameter of less than 200 nm FWHM. The setup also includes a six-circle, high-precision sample diffractometer and custom-made sample holder. They demonstrated the nanodiffraction capabilities in experiments using scattering from individual triclinic tin oxide (Sn_2O_3) nanobelts with cross-section down to 24 nm × 10 nm. Working at HASYLAB and ESRF, Jarre et al. [13] describe the design, fabrication and characterization of X-ray waveguides for use as ultra-narrow X-ray slits. By combining waveguides with K–B prefocusing mirrors, they report X-ray beams with cross-section as small as 25 nm FWHM. It should be noted that individual objects can be probed using X-ray beams larger than the nanostructure size as long as sufficient scattered intensity and separation between objects are achieved. Using beam sizes in the range ~1–6 μm at the ESRF, studies have been carried out on rolled-up single crystal GaAs/InAs nanotubes [14] and on single-walled carbon nanotubes [15]. At a high-energy ESRF three-dimensional X-ray diffraction (3DXRD) beamline (ID11), diffraction peaks from individual grains as small as 70 nm can be measured [4]. Most focused X-ray facilities utilize monochromatic X-ray beams, and include both nanodiffraction and nanofluorescence mapping capabilities.

At the APS sector 34, we have initiated nanoscience experiments to characterize the local lattice structure from spatially-resolved regions of individual 1D structures. In our initial experiments, we have used hexagonal ZnO and cubic tin-doped indium oxide (ITO) materials fabricated in various nanoshapes: rods, belts, combs and tapered styluses. As described in the Introduction, our X-ray microscopy beamline allows the user to select either a polychromatic or a monochromatic beam. Unlike monochromatic facilities, white-beam diffraction yields a full Laue pattern for all sample orientations, and hence eliminates the need for a sample rotation stage and angular scans. Although the beam diameter is typically ~500 nm during routine operation, beams as small as 90 nm have been demonstrated on this beamline [16].

ZnO and tin-doped indium oxide (ITO) nanostructures have generated tremendous research interest due to their unique optical, electrical, mechanical and chemical properties [17,18]. Applications such as optoelectronic devices or ultra-sensitive sensors will require an understanding of how the device morphology, lattice structure and doping levels control these properties. Here, we demonstrate how X-ray microfluorescence and nanodiffraction can be used to study the growth of individual ZnO nanorods. ZnO is a direct, wide-bandgap material and is also piezoelectric. It can be synthesized in a wide variety of morphologies, and is a leading candidate material for many nanodevice applications including surface acoustic wave and UV lasing devices [18,19].

The ZnO nanorods were synthesized by Ge-catalyzed crystal growth as described by Pan [20]. Spherical Ge catalyst nanoparticles serve to nucleate and direct the ZnO nanorod growth process. Since oxide nanowires are commonly grown using metal catalysts (e.g. Au, Fe), very few studies of growth mechanisms or interfacial reactions associated with semiconductor catalyst particles such as Ge have been carried out. The diameters of the Ge spheres were usually in the range 1–4 μm while the ZnO rod diameter was generally less than a micron. Fig. 2a shows an optical image of a Ge-catalyzed ZnO nanorod mounted on a TEM grid. Two other smaller rods are in this general area, but are out of focus. The catalyst particle in Fig. 2a was first located with the X-ray microbeam by mapping the intensity of the Ge–K fluorescence as the sample is translated over a 2D area in 1 μm steps. A monochromatic beam just above the K-edge (11.1 keV) was used for this scan to reduce background scattering. The resulting map is shown in Fig. 2b. No evidence for Ge content was seen in the ZnO rod.

Once the spherical Ge particle was located using fluorescence, Laue diffraction patterns from the associated ZnO rod were obtained using a polychromatic microbeam and the CCD area detector. A typical pattern is shown in Fig. 3a. Indexation of the diffraction peaks revealed that the ZnO rod has a hexagonal Wurtzite structure with the [0001] direction along the growth axis. Laue patterns were then collected while the sample was translated in a two-dimensional scan covering a 20 μm × 10 μm area with a step size of 0.5 μm. Diffraction

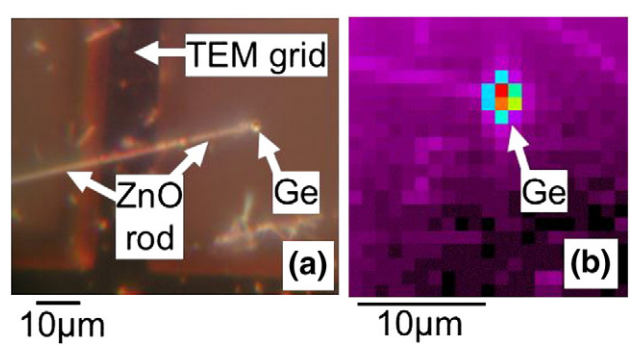

Fig. 2. (a) Optical image of Ge-catalyzed ZnO nanorod mounted on a TEM grid. The long (>50 μm) ZnO rod is capped by a ~spherical Ge particle. (b) X-ray microfluorescence area map used to locate the same Ge catalyst particle shown in panel a. Pixel size is 1 μm. The ZnO rod does not appear since it does not incorporate Ge during growth.

images collected from the Ge catalyst particle showed many superimposed Laue patterns and strong fluorescence background, while images collected from the ZnO rods showed a single-crystal Wurtzite pattern. The microdiffraction information from the 2D area scan can be displayed in several forms. Fig. 3b shows the ZnO lattice orientations as standard hexagonal *c*-axis and *a*-axis pole figure representations. For each spatial position in the area scan, a red marker is added to the stereographic projections to indicate the direction of normal to the ZnO(0001) and the ZnO{1000} planes respectively. The center of each projection corresponds to the surface normal of the sample TEM grid. These pole figures show three distinct crystal orientations, but do not provide any spatial information.

The spatial location of the different lattice orientations is shown in a ZnO(0001) orientation map in Fig. 4. This map is generated by assigning a color to each pixel in the area scan based on the direction of the ZnO *c*-axis at that location. The color legend is shown on the right (note: 2D orientation maps are commonly used to display electron back-scatter diffraction (EBSD) results and the same concept is used here). The directions and the shapes of three ZnO nanorods are clearly seen. Each rod is a hexagonal single crystal with some small curvature presumably associated with a gradual bending of the rod. The *c*-axis is aligned with the rod length in each case. The larger rod labeled ZnO-1 is growing out from the Ge particle. The Ge diffraction images showed the superposition of several different orientations at every position, indicating that the catalyst particle is a fine-grain polycrystal. The Laue patterns

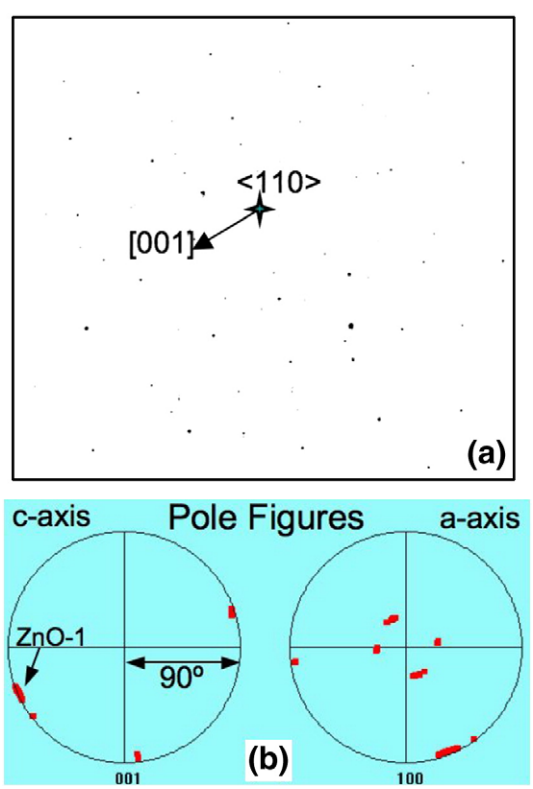

Fig. 3. (a) Typical Laue diffraction pattern from an individual hexagonal ZnO nanorod. (b) Hexagonal *c*-axis and *a*-axis pole figures generated by scanning in the area of a few ZnO nanorods.

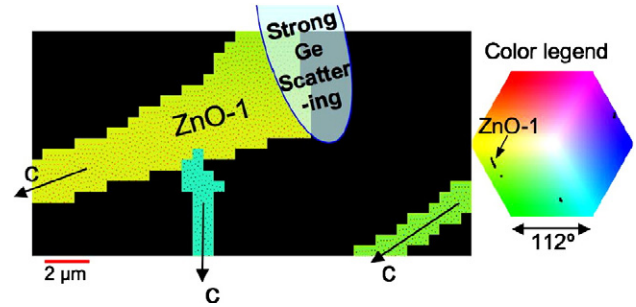

Fig. 4. Spatially-resolved orientation map where the colored pixels indicate nonzero ZnO diffracted intensity is observed (i.e. incident microbeam hits a nanorod). Three single-crystal ZnO nanorods are observed. Color indicates the direction of the ZnO[0001] axis as a function of position using the color legend on the right and the pole figure data from Fig. 3b. (For interpretation of the references to colour in this figure legend, the reader is referred to the web version of this article.)

obtained from the region near the Ge–ZnO interface showed no signs of any particular orientation relationship between the ZnO rod and the Ge particle. Thus, the ZnO rod does not grow epitaxially. Instead, our observations are consistent with the suggestion by Pan [20] that the rods grow by the vapor–liquid–solid (VLS) crystal growth mechanism. Based on the fact that the Ge–Zn phase diagram exhibits a eutectic reaction at 394 °C and 94 atom% Zn, it is believed that the Ge particles are in the liquid state at growth temperatures (500–600 °C). Our observations are consistent with this description.

We have measured X-ray microfluorescence and microdiffraction from ZnO and ITO nanostructures in several other geometries, including nanowires mounted across electrical contacts, tapered styluses, and cross-section slices extracted by focused ion-beam (FIB) milling. The ability of X-ray microdiffraction to quantitatively characterize microstructures with high angular and strain resolution will likely provide valuable information to complement more qualitative, higher spatial resolution results from other techniques. For example, although not demonstrated here, X-ray microdiffraction yields the local strain tensor with resolution $\Delta d/d \sim 10^{-4}$. We plan to use this capability to measure the doping- and size-dependent mechanical response of individual piezoelectric nanowires as a function of applied voltage. Clearly, as beam sizes decrease and facilities are further developed, X-ray nanodiffraction will enable many new opportunities for fundamental nanoscience research.

3. 2D: deposited films

Conventional X-ray diffraction measurements with ~mm-size beams have played an important role in advancing our fundamental understanding of thin film growth for many decades. The ability to measure microstructural aspects such as epitaxial film/substrate relationships, residual thermal stresses and thickness control has made X-ray diffraction (XRD) a traditional tool for characterizing thin film and layered systems. Synchrotron microbeams now enable a more complete structural description of thin film systems. Film inhomogeneities often play an important role in determining the physical

properties and microdiffraction can now provide a spatially-resolved description of the local variations in orientation and strain. In many applications ranging from corrosion-resistant coatings to magnetic recording media, grain size and texturing in films can strongly affect performance.

Synchrotron-based microdiffraction has recently provided many new results in a range of thin film studies. For example, deposited layers in electronic devices are often patterned to produce localized features. The dimensions and strain within such features are critical to device operation. Cai et al. [21] used X-ray microdiffraction to map the spatial variation of the lattice strain and multilayer thicknesses in InGaAsP optoelectronic devices produced by a selective area growth technique. Do et al. [22] developed a method to image the polarization domains in epitaxial ferroelectric PZT films and used this approach to investigate how polarization fatigue depends on the applied switching conditions. A large number of research groups have investigated plastic deformation, void formation, and strain enhancement associated with electromigration in metal interconnects [23–28]. In these studies, quantitative *in-situ* studies of the microstructural evolution were enabled by the penetration of hard X-rays through the oxide passivation layer. Other microbeam studies of electronic thin film systems have used X-ray penetration to study the epitaxial relationships between films and the underlying substrates. Several researchers have mapped the crystallographic tilts and strain variations across the wing regions in epitaxial GaN films grown by lateral overgrowth methods [29–31]. Here, we will describe how X-ray microdiffraction studies of epitaxial oxide films deposited on roll-textured metal foils help guide the development of high-T_c superconducting wires with enhanced current-carrying capabilities [32].

Following the discovery of high-T_c oxide superconductors over twenty years ago, considerable research worldwide has been directed towards achieving long-length, high critical-current (J_c) wires. Since early work revealed that high-angle boundaries in materials such as YBaCuO suppress J_c by orders of magnitude, techniques for fabricating highly-aligned coated conductors have been developed [33]. One such technique is now referred to as Rolling-Assisted Biaxially-Textured Substrates (RABiTS) [34,35]. In this approach, oxide buffer layers (e.g. CeO_2 and YSZ) and then superconducting films are deposited epitaxially on recrystallization-textured metal (e.g. Ni) tapes. The oxide layers are crystallographically aligned by epitaxy on the textured substrate and the critical current density depends strongly on the degree of alignment [33,35,36]. However, conventional X-ray rocking curves (see Fig. 2 of Ref. [35]) have shown that the different layers in these composite materials exhibit different degrees of mosaic spread. Moreover, the degree of alignment depends on growth conditions. We have employed X-ray microdiffraction in order to better understand the detailed mechanisms controlling epitaxial growth and orientation control in oxide films on textured Ni substrates [32]. Because the X-ray beam simultaneously probes both the film layers and the substrate and possesses high angular resolution, it is an ideal tool for mapping local epitaxial relationships on a grain-by-grain basis.

The samples were 0.5 μm thick CeO_2 oxide films grown by pulsed laser ablation (PLD) on highly-textured 50 μm thick Ni substrates at temperatures in the range 450–785°C. Grain sizes in the metal foil were typically ~50 μm laterally. Using a polychromatic microbeam, Laue diffraction at each position showed an intense Ni pattern and a separate, weaker CeO_2 pattern. Since both structures are cubic, the fact that the patterns were not superimposed reveals that the film is not exactly aligned with the substrate. Instead, systematic crystallographic tilts between the film and substrate are present.

Fig. 5 shows typical out-of-plane and in-plane orientation maps for the Ni substrate and the CeO_2 film. The pole figure on the left beneath each orientation map shows the standard full stereographic representation with 90° between the center of the plot (out-of-plane direction) and the large circle (in-plane directions). The strong [001<100> Ni cube texture and a 45° in-plane plane rotation of the film are evident. The pole figure on the right beneath each map shows an enlargement (labeled 'zoom') of the angular region within the red circles, now spanning only 5.3° between the center and the circle edge. The color for each pixel in the orientation maps is determined by superimposing the zoomed pole figures onto the red–green–blue hexagonal color legends. The substrate and film grain morphologies and colors appear very similar in the maps due to the approximate epitaxial relation. However, quantitative analysis of the orientation data shown in figures such as these reveals two important features. First, each Ni grain is essentially a single-crystal with very small angular mosaic spread. In contrast, there is much greater subgrain angular variation for the CeO_2 film (i.e. 'fuzzy' spots in zoomed pole figure). This local epitaxial disorder is likely due to multiple nucleation sites within each Ni grain and may provide beneficial superconductor flux pinning sites. Second, the position of the CeO_2 out-of-plane (001) pole for any particular grain is tilted slightly closer to the surface normal than the pole for the underlying Ni grain. This crystallographic tilting results in a sharper out-of-plane texture for the film than for the substrate. A quantitative analysis of the lattice tilts revealed a linear relation between the tilt of the heteroepitaxial layer and the local miscut angle of a particular substrate grain. These results are in qualitative agreement with a geometrical model for epitaxial growth proposed by Nagai [37]. This atomistic model assumes that heteroepitaxial films are epitaxially strained to match the substrate lattice at surface ledges, but relax to their unstrained value as growth proceeds across the ledge [32].

X-ray microdiffraction has been used to investigate other oxide layers for superconducting applications. Recent microdiffraction work by Specht et al. [38] has extended the studies of the YBaCuO layer in RABiTS samples. Using a novel analysis algorithm based on a Hough transform, they investigated orientation variations in YBaCuO films and correlated the results with the size and tilt of the Ni grains. In general, the microdiffraction experiments demonstrate how spatially-resolved results provide new insight into growth mechanisms and suggest techniques for controlling film textures through the selection of heteroepitaxial systems with particular lattice mismatch. For superconducting applications, the sharper film

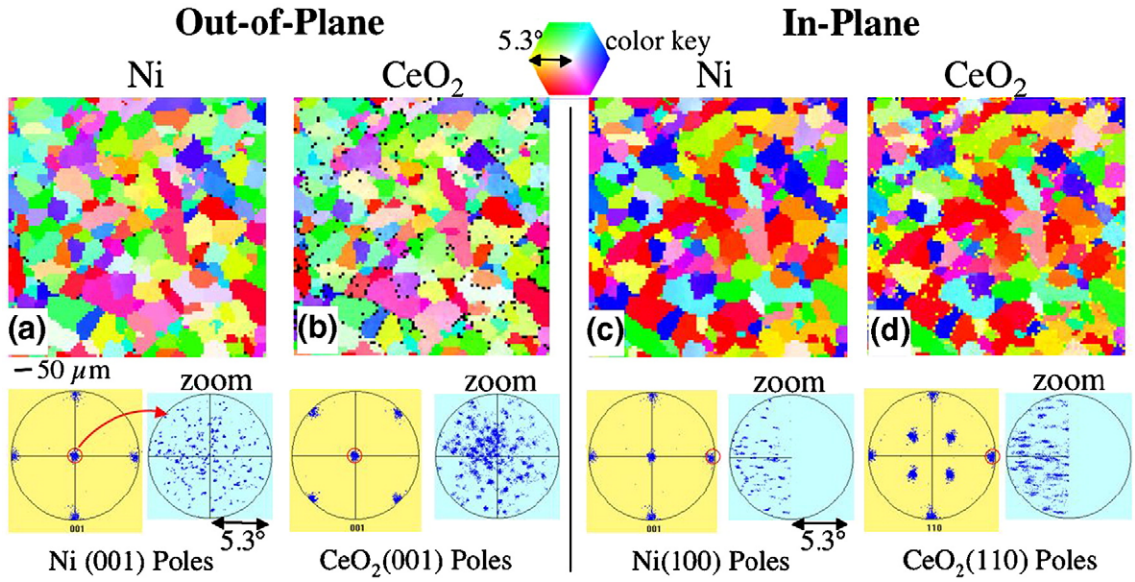

Fig. 5. Top figures show orientation maps of Ni substrate and CeO_2 film with out-of-plane Ni(001) and CeO_2(001) maps on the left and in-plane Ni(100) and CeO_2 (110) maps on the right. Bottom figures show corresponding pole figures as both full 90° stereographic projection and as a zoomed projection with 5.3° angular range.

texture leads to larger percolative regions with boundaries <~5° and thus enhanced critical current densities [32]. The tilt mechanisms described here should be relevant to many other heteroepitaxial material systems such as thermal barriers, solar cells or corrosion-resistant coatings.

4. 3D: structure and evolution of polycrystals

X-ray penetration into most materials is deep when compared with electron probes. As described in the Introduction, the ability to spatially reconstruct depth-resolved X-ray scattering has enabled recent progress in the development of 3D X-ray microscopy techniques [3–6,11,39]. This ability to non-destructively map the 3D structure and evolution *inside* polycrystalline materials with high-resolution was not previously possible. Electron microscopes that combine focused ion-beam milling and electron backscatter diffraction (EBSD) scanning are now highly-automated and can provide high-resolution 3D structural maps [8–10]. However, the sample is destroyed during serial sectioning, precluding studies of structural evolution. In contrast, neutron beams penetrate large distances in most materials, but the relatively large source size (i.e. low brilliance) prohibits focusing with both high intensity and small beam size. Thus, X-ray microscopy will play a particularly important role in high-resolution studies of dynamic processes in 3D materials.

3D X-ray microdiffraction has already enabled new scientific results involving several classic fields of materials processing. For example, understanding the fundamental processes controlling elastic and plastic strains generated by deformation represents a long-standing challenge in materials science. It is known that deformation in ductile metals often results in ~micron-size dislocation cell structures in which regions of relatively perfect material are separated by dislocation-rich walls [40]. However, the dislocation interactions responsible for cell formation are not understood. Levine et al. [41] have used scanning monochromatic 3D X-ray microdiffraction [42] to measure the internal elastic strains in individual dislocation cells in deformed copper. Their results were consistent with a "composite model" of deformation based on interactions between elastically-hard cell walls and softer cell interiors [40]. They succeeded in identifying the predicted internal back-stresses within individual cells due to the original compressive or tensile deformation. Jakobsen et al. [43] have studied the dislocation self-organization processes in deformed metals using monochromatic, high-energy X-ray microdiffraction. They identify diffraction spots arising from different subgrains within an individual grain separated by regions of larger dislocation density and interpret their results in terms of the composite model. Further, they observe unexpected intermittent dynamics during deformation in which more perfect regions appear and disappear while surrounded in a sea of dislocations. In other studies of deformation in metals, Yang et al. [44] have examined the microstructure under microindents in single-crystal Cu. Measurements of local lattice rotations were used to generate spatially-resolved 3D maps of the geometrically-necessary dislocation (GND) densities. Again, dislocation patterning and cell wall structures were experimentally observed. These high-resolution, quantitative 3D results for a well-defined deformation geometry will provide the experimental input needed for testing predictions of computer simulations of crystal plasticity. Clearly, the recent studies of 3D deformation microstructures are already providing valuable new insight into the complex materials processes associated with dislocation patterning.

A second major field where 3D microscopy is now poised to address long-standing material questions involves studies of grain nucleation and growth during recrystallization and thermal annealing. Using the 3D X-ray diffraction (3DXRD) microscope at the ESRF, Schmidt et al. [45,46] tracked the size

and shape of a single grain during recrystallization of deformed Al. They find that, rather than a steady increase in grain size and shape, grain growth proceeds in abrupt movements of different boundary segments. They believe that irregular movements are due to inhomogeneities such as variations in dislocation density or different misorientation angles for Al boundaries. In a materials system of large practical importance, Offerman et al. [47,48] have used the 3DXRD microscope to study the kinetics of the austenite to ferrite phase transformation in carbon steel. By observing individual grains, they gained new insights into the nucleation and growth of the ferrite grains. For example, they concluded that the activation energy for ferrite nucleation is ~100 times smaller than the value expected from thermodynamic models. Detailed experimental measurements such as these are important for providing guidance in the development of more accurate models of nucleation and grain growth.

At the APS, we have used *in-situ* polychromatic 3D microdiffraction to investigate 3D grain growth in polycrystalline Al [49]. Since controlling grain sizes and texture is an important goal of thermal processing, grain growth in bulk materials has been studied extensively for well over a century. Now, X-ray microscopy allows us to non-destructively image the evolution of individual grains and grain boundaries in the interior of polycrystals. As shown schematically in Fig. 6a, the X-ray microbeam was scanned near the edge of a sample of hot-rolled (200°C) 1xxx series aluminum (~1% Fe,Si) obtained from Alcoa. The DAXM (Pt wire) technique was used to map the orientation of each 1 μm^3 voxel in a particular 10 μm × 10 μm × ~100 μm volume. The diffraction peaks in the reconstructed patterns were sharp, indicting significant recrystallization during hot-rolling (200 °C). As shown in Fig. 6b where different colors represent different grains, the typical grain size was initially of order ~5–10 μm. The sample was then annealed, cooled to room temperature and the microstructure for the same volume was remeasured. Measurements after annealing steps at successively higher temperatures (350°, 355°, 360°, and 365 °C) resulted in 3D orientation maps corresponding to 'snapshots' of the evolution of the grains inside the sample during thermal annealing. Fig. 6(c–f) shows the evolution of the microstructure within a single 2D slice as the grains grow larger with increasing temperature. Software has been developed to analyze grain boundary misorientations and boundary planes, identify boundary types such as twins or coincidence orientations, and generate Rodrigues space representations. It is important to note that, since point-to-point data with high angular resolution is obtained, we are also able to map local imperfections such as the GND density. The energy associated with such intragranular defects can represent an important driving force for boundary migration and must be considered in theoretical models. Experimentally, we observe both high-angle and low-angle boundary migration. These measurements demonstrate that previously unavailable, non-destructive, high-resolution 3D grain growth measurements can now be obtained. This type of data represents the input needed for quantitatively testing the validity of theories and computer models of 3D grain growth in polycrystal materials, and these tests are currently in progress.

5. Conclusions and future directions

Advances in high-brightness synchrotron sources and precision X-ray optics have enabled rapid progress in the development of spatially-resolved X-ray microscopy techniques. Here, we have described the scanning, polychromatic (white) microdiffraction facility developed at the XOR-UNI beamline 34ID at the APS. This beamline uses Kirkpatrick–Baez (K–B) mirrors to focus undulator radiation to a typical beam diameter of ~0.5 μm, and can be operated in polychromatic (white) or monochromatic modes. In polychromatic mode, Laue diffraction images are analyzed to obtain the local crystal symmetry, lattice orientation, and the strain tensor. The fact that white Laue diffraction does not require sample rotations in order to excite Bragg peaks is a significant advantage whenever the sample crystal structure or orientation is not known. Once a Laue pattern is indexed, monochromatic mode provides absolute values for the local lattice parameters. Submicron spatial resolution is obtained in all 3 dimensions. The beam diameter determines the resolution laterally, while a differential-aperture X-ray microscopy (DAXM) technique has been developed to achieve submicron spatial-resolution along the direction of the beam path. It is important to note that the spatial resolution represents a point-to-point measurement from

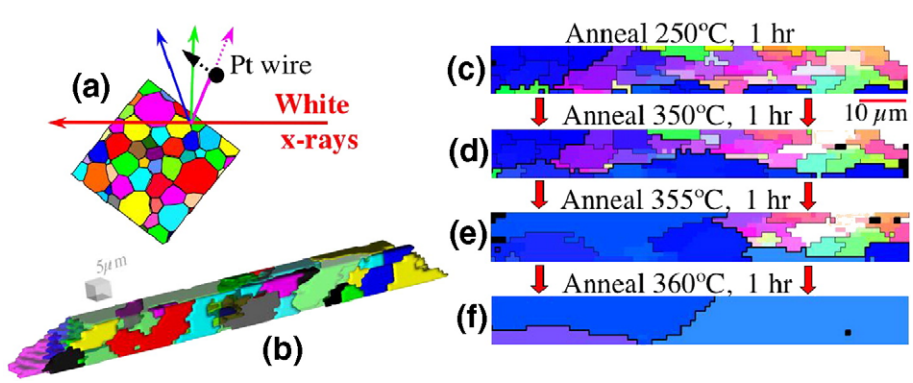

Fig. 6. (a) Schematic of 3D microscopy of polycrystal Al. (b) Initial 3D orientation image of hot-rolled (200 °C) Al after a low temperature anneal of 250 °C for 1 h. Colors indicate different grains. (c–f) Microstructure in a 2D slice after annealing at successively higher temperatures (350 °C, 355 °C, 360 °C) for 1 h each. (For interpretation of the references to colour in this figure legend, the reader is referred to the web version of this article.)

each voxel, not simply the ability to measure scattering from a single small crystallite or nanostructure. Thus, intragranular as well as intergranular microstructural measurements are possible. The angular resolution for measurements of Bragg diffraction peaks is ~0.01° and the strain resolution is $\Delta d/d \sim 10^{-4}$.

X-ray microscopy can be used to obtain unique, quantitative structural information and new insight for a wide variety of materials. In this paper, examples illustrating the usefulness of spatially-resolved X-ray diffraction were drawn from the general classes of 1D, 2D and 3D material systems. The ability to study individual 1D nanostructures is a direct result of improved focusing of intense X-ray beams into small diameters. We have measured X-ray microfluorescence and microdiffraction orientation maps from individual hexagonal ZnO nanorods and the associated polycrystalline Ge catalyst particles. The observations were consistent with a vapor–liquid–solid (VLS) crystal growth mechanism for this system. For 2D systems such as deposited films or multilayer materials, X-ray microdiffraction enables the simultaneous measurements from both the substrate and the film layers. We illustrated the benefits of this capability in a study of epitaxial oxide films grown on highly-textured Ni substrates for superconducting applications. This study revealed systematic crystallographic tilts of the oxide film away from the exact epitaxial orientation, leading to a better understanding of how to control texture in epitaxial films. For 1D and 2D systems, electron probes can often provide complementary detailed structural measurements. However, this is not true for 3D material systems, and it is likely that spatially-resolved 3D X-ray microscopy will provide the most unique opportunities for new material investigations. Investigations have been initiated to quantitatively study the self-organized dislocation cell structures that result from plastic deformation. Here, we illustrated 3D X-ray microscopy with orientation maps showing snapshots of the evolution of the 3D grain morphology in polycrystalline aluminum during thermal annealing. Time-resolved 3D characterizations are sometimes referred to as 4D X-ray microscopy to highlight the ability to carry out dynamic studies [4].

As progress in X-ray sources, X-ray optics, area detectors and analysis software continues, the field of X-ray microscopy will continue to grow. Clearly, beam sizes for both monochromatic and polychromatic beams will continue to shrink. We have demonstrated polychromatic focusing to ~90 nm using K–B mirrors on the XOR-UNI beamline APS [16]. Using a 1 km long beamline at SPring-8 and precision K–B mirrors, Mimura et al. report focusing to a beam size of 25 nm at 15 keV [50]. Nanoprobe beamlines now under development at the APS and ESRF include focusing to ~30 nm [4,51,52]. Advances will continue for years to come; future radiation sources, such as those based on energy recovery linacs (ERL) [53], will provide smaller inherent source sizes and hence enable more X-rays to be focused into even smaller beams.

Smaller, brighter beams will, in turn, enable more detailed investigations of new material systems of interest for both fundamental and technological considerations. In principle, spatially-resolved X-ray diffraction patterns can be obtained from any material that scatters X-rays, including distorted single-crystals, films, multi-phase composites, biological materials, minerals, elastically and plastically deformed materials, nanostructures, and even amorphous materials. In addition, although not discussed here, other X-ray tools can be incorporated with microdiffraction into the same beamline facility. By combining spatially-resolved X-ray diffraction, fluorescence, spectroscopy (EXAFS, XANES), and tomography, more complete material descriptions will be possible. Finally, we note that many of the concepts discussed here for X-rays, including focusing with K–B mirrors, are applicable to neutrons [54]. More intense, penetrating neutron beams are now available at the Spallation Neutron Source (SNS). The development of a 3D neutron microscopy facility would allow scattering probes using electrons, X-rays and neutrons to cover the complete range from nanometer to centimeter length scales with overlapping spatial resolution.

Acknowledgements

Research sponsored by the Division of Materials Sciences and Engineering, U.S. Department of Energy, Office of Science under contract with UT-Battelle, LLC. UNI-CAT/XOR supported by ORNL, UIUC-MRL, NIST, UOP and DOE-BES Office of Science. Use of the APS was supported by the U.S. Department of Energy, Office of Basic Energy Sciences, under Contract No. DE-AC02-06CH11357.

References

[1] G.E. Ice, X-Ray Spectom. 26 (1997) 315.
[2] C. Riekel, Rep. Prog. Phys. 63 (2000) 233.
[3] B.C. Larson, B. Lengeler, High-Resolution Three-Dimensional X-Ray Microscopy, Mater. Res. Soc. Bull. 29 (2004) 152.
[4] D. Juul Jensen, E.M. Lauridsen, L. Margulies, H.F. Poulsen, S. Schmidt, H.O. Sørensen, G.B.M. Vaughan, Materials Today 9 (2006) 18.
[5] H.F. Poulsen, Three-Dimensional X-Ray Diffraction microscopy: Mapping polycrystals and their dynamics, Springer, Berlin, Germany, 2004.
[6] G.E. Ice, B.C. Larson, W. Yang, J.D. Budai, J.Z. Tischler, J.W.L. Pang, R.I. Barabash, W. Liu, J. Synchrotron Radiat. 12 (2005) 155.
[7] N. Tamura, H.A. Padmore, J.R. Patel, Mater. Sci. Eng. A 399 (2005) 92.
[8] J.E. Spowart, Scr. Mater. 55 (2006) 5.
[9] M. Uchic, M.A. Groeber, D.M. Dimiduk, J.P. Simmons, Scr. Mater. 55 (2006) 23.
[10] D.J. Rowenhorst, A. Gupta, C.R. Feng, G. Spanos, Scr. Mater. 55 (2006) 11.
[11] B.C. Larson, W. Yang, G.E. Ice, J.D. Budai, J.Z. Tischler, Nature 415 (2002) 887.
[12] Y. Xiao, Z. Cai, B. Lai, Nanotechnology 16 (2005) 1754.
[13] A. Jarre, J. Seeger, C. Ollinger, C. Fuhse, C. David, T. Salditt, J. Appl. Phys. 101 (2007) 054306.
[14] B. Krause, C. Mocuta, T.H. Metzger, Ch. Deneke, O.G. Schmidt, Phys. Rev. Lett. 96 (2006) 165502.
[15] V. Pichot, M. Burghammer, S. Badaire, C. Zakri, C. Riekel, P. Poulin, P. Launois, Europhys. Lett. 79 (2007) 46002.
[16] W.J. Liu, G.E. Ice, J.Z. Tischler, A. Khounsary, C. Liu, L. Assoufid, A.T. Macrander, Rev. Sci. Instrum. 76 (2005) 113701.
[17] Z.W. Pan, Z.R. Dai, Z.L. Wang, Science 291 (2001) 1947.
[18] Y.W. Heo, D.P. Norton, L.C. Tien, Y. Kwon, B.S. Kang, F. Ren, S.J. Pearton, J.R. LaRoche, Mater. Sci. Eng. R 47 (2004) 1.
[19] L. Schmidt-Mende, J.L. MacManus-Driscoll, Materials Today 10 (2007) 40.
[20] Z.W. Pan, S. Dai, C.M. Rouleau, D.H. Lowndes, Angew. Chem. Int. Ed. 44 (2005) 274.

[21] Z.-H. Cai, W. Rodrigues, P. Ilinski, D. Legnini, B. Lai, W. Yun, E.D. Isaacs, K.E. Lutterodt, J. Grenko, R. Glew, S. Sputz, J. Vandenberg, R. People, M.A. Alam, M. Hybertsen, L.J.P. Ketelsen, Appl. Phys. Lett. 75 (1999) 100.
[22] D.H. Do, P.G. Evans, E.D. Isaacs, D.M. Kim, C.B. Eom, E.M. Dufresne, Nat. Mater. 3 (2004) 365.
[23] H.-K. Kao, G.S. Cargill III, F. Giuliani, C.-K. Hu, J. Appl. Phys. 93 (2003) 2516.
[24] A.T. Wu, K.N. Tu, J.R. Lloyd, N. Tamura, B.C. Valek, C.R. Kao, Appl. Phys. Lett. 85 (2004) 2490.
[25] R.I. Barabash, G.E. Ice, N. Tamura, B.C. Valek, J.C. Bravman, R. Spolenak, J.R. Patel, Microelectron. Eng. 75 (2004) 24.
[26] X. Zhang, H. Solak, F. Cerrina, B. Lai, Z. Cai, P. Ilinski, D. Legnini, W. Rodrigues, Appl. Phys. Lett. 76 (2000) 315.
[27] A.S. Budiman, W.D. Nix, N. Tamura, B.C. Valek, K. Gadre, J. Maiz, R. Spolenak, J.R. Patel, Appl. Phys. Lett. 88 (2006) 233515.
[28] A. Lee, W. Liu, C.E. Ho, K.N. Subramanian, J. Appl. Phys. 102 (2007) 053507.
[29] R.I. Barabash, C. Roder, G.E. Ice, S. Einfeldt, J.D. Budai, O.M. Barabash, S. Figge, D. Hommel, J. Appl. Phys. 100 (2006) 053103.
[30] D. Lubbert, P. Mikulík, P. Pernot, L. Helfen, M.D. Craven, S. Keller, S. DenBaars, T. Baumbach, Phys. Status Solidi a 203 (2006) 1733.
[31] M. Drakopoulos, M. Laugt, T. Riemann, B. Beaumont, P. Gibart, Phys. Status Solidi B 243 (2006) 1545.
[32] J.D. Budai, W. Yang, N. Tamura, J.S. Chung, J.Z. Tischler, B.C. Larson, G.E. Ice, C. Park, D.P. Norton, Nat. Mater. 2 (2003) 487.
[33] S.R. Foltyn, L. Civale, J.L. MacManus-Driscoll, Q.X. Jia, B. Maiorov, H. Wang, M. Maley, Nat. Mater. 6 (2007) 631.
[34] J.D. Budai, R.T. Young, B.S. Chao, Appl. Phys. Lett. 62 (1993) 1836.
[35] D.P. Norton, A. Goyal, J.D. Budai, D. Christen, D. Kroeger, E.D. Specht, Q. He, B. Saffian, M. Paranthaman, C. Klabunde, D. Lee, B. Sales, F. List, Science 274 (1996) 755.
[36] D.P. Norton, D.H. Lowndes, J.D. Budai, D.K. Christen, E.C. Jones, K.W. Lay, J.E. Tkaczyk, Appl. Phys. Lett. 57 (1990) 1164.
[37] H. Nagai, J. Appl. Phys. 45 (1974) 3789.
[38] E.D. Specht, A. Goyal, W. Liu, J. Mater. Res. 22 (2007) 664.
[39] J.D. Budai, W. Yang, B.C. Larson, J.Z. Tischler, W. Liu, G.E. Ice, in: S.R. Bhatia, P.G. Khalifah, D.J. Pochan, P.G. Radaelli (Eds.), Neutron and X-Ray Scattering as Probes of Multiscale Phenomena, Boston, U.S.A., Nov. 28–Dec. 3, 2004, Materials Research Society Symposium Proceedings 840, 2004, Q7.1.
[40] H. Mughrabi, T. Ungar, Nat. Mater. 5 (2006) 601.
[41] L.E. Levine, B.C. Larson, W. Yang, M.E. Kassner, J.Z. Tischler, M.A. Delos-Reyes, R.J. Fields, W. Liu, Nat. Mater. 5 (2006) 619.
[42] W. Yang, B.C. Larson, G.E. Ice, J.Z. Tischler, J.D. Budai, K.-S. Chung, W.P. Lowe, Appl. Phys. Lett. 82 (2003) 3856.
[43] B. Jakobsen, H.F. Poulsen, U. Lienert, J. Almer, S.D. Shastri, H.O. Sørensen, C. Gundlach, W. Pantleon, Science 312 (2006) 889.
[44] W. Yang, B.C. Larson, G.M. Pharr, G.E. Ice, J.D. Budai, J.Z. Tischler, W. Liu, J. Mater. Res. 19 (2004) 66.
[45] S. Schmidt, S.F. Nielsen, C. Gundlach, L. Margulies, X. Huang, D. Juul Jensen, Science 305 (2004) 229.
[46] H.O. Sørensen, B. Jakobsen, E. Knudsen, E.M. Lauridsen, S.F. Nielsen, H.F. Poulsen, S. Schmidt, G. Winther, L. Margulies, Nucl. Instrum. Methods Phys. Res. B 246 (2006) 232.
[47] S.E. Offerman, N.H. van Dijk, J. Sietsma, S. Grigull, E.M. Lauridsen, L. Margulies, H.F. Poulsen, M.Th. Rekveldt, S. van der Zwaag, Science 298 (2002) 1003.
[48] N.H. van Dijk, S.E. Offerman, J. Sietsma, S. van der Zwaag, Acta Mater. 55 (2007) 4489.
[49] J.D. Budai, W. Yang, B.C. Larson, J.Z. Tischler, W. Liu, H. Weiland, G.E. Ice, Mat. Sci. Forum 467–470 (2004) 1373.
[50] H. Mimura, H. Yumoto, S. Matsuyama, Y. Sano, K. Yamamura, Y. Mori, M. Yabashi, Y. Nishino, K. Tamasaku, T. Ishikawa, K. Yamauchi, Appl. Phys. Lett. 90 (2007) 051903.
[51] J. Maser, R. Winarski, M. Holt, D. Shu, C. Benson, B. Tieman, C. Preissner, A. Smolyanitskiy, B. Lai, S. Vogt, G. Wiemerslage, G.B. Stephenson, Proceedings of the 8th International Conference on X-ray Microscopy, Himeji, Japan, July 2005, Institute of Pure and Applied Physics Conference Series, vol. 7, 2006, p. 26.
[52] C.M. Kewish, L. Assoufid, A.T. Macrander, Jun Qian, Appl. Opt. 46 (2007) 2010.
[53] Q. Shen, D.H. Bilderback, K.D. Finkelstein, I. Bazarov, S. Gruner, J. Phys. IV 104 (2003) 21.
[54] G.E. Ice, C.R. Hubbard, B.C. Larson, J.W.L. Pang, J.D. Budai, S. Spooner, S.C. Vogel, R.B. Rogge, J.H. Fox, R.L. Donaberger, Mater. Sci. Eng. A 437 (2006) 120.